Influence of the shell structure of colliding nuclei in fusion-fission reactions

V. L. Litnevsky* and V. V. Pashkevich†
Bogoliubov Laboratory of Theoretical Physics, JINR, Dubna, Russia

G. I. Kosenko‡
Omsk State University, Omsk, Russia

F. A. Ivanyuk§
Institute for Nuclear Research, Kiev, Ukraine

(Received 14 August 2011; revised manuscript received 23 January 2012; published 9 March 2012)

We describe the fusion-fission processes within a two-stage reaction model. In the first stage (the approach phase) we calculate the properties of the system at the touching point. In the second stage we describe the evolution of the compact system. It is assumed that in the approach process the colliding ions are oriented "nose to nose"; i.e., their symmetry axes coincide. The distributions at the touching point obtained at the first step are used as the initial conditions for the evolution of a compact system. Both the approach phase and the evolution of the compact system are described in terms of Langevin equations for the collective coordinates (deformation parameters). At both stages the shell structure of the colliding ions and that of the compound nucleus are taken into account. Within this model we obtain information on the touching probability and on the observables measured in the fusion-fission reactions (mass and energy distributions of the fission fragments, the touching and fusion cross sections, and the evaporation residue cross sections). Results obtained for the reactions $^{16,18}\mathrm{O} + {}^{208}\mathrm{Pb} \rightarrow {}^{224,226}\mathrm{Th}$ and $^{48}\mathrm{Ca} + {}^{208}\mathrm{Pb} \rightarrow {}^{256}\mathrm{No}$, involving nuclei that are spherical in their ground state, are compared with the available experimental data.

DOI: 10.1103/PhysRevC.85.034602 PACS number(s): 25.70.Jj, 24.10.−i, 21.60.Cs

I. INTRODUCTION

One of the most challenging problems of heavy-ion physics is the theoretical description of fusion-fission reactions. By comparing the calculated and experimental results one can check our understanding of the reaction mechanism of heavy-ion collisions.

According to Bohr's compound-nucleus concept "fusion" means the formation of the compound nucleus around the spherical shape, and then fission can proceed independently from the formation process. Nowadays, however, in the description of fusion-fission reactions one often includes all intermediate processes which take place in heavy-ion collisions. In the present paper we consider the fusion-fission process as the approach of the nuclei in the entrance channel, formation of a compact system, and the fission process. The concept of "fission" is not confined to fission from the spherical compound nucleus but includes all the binary decays of the compact system.

Though the approach process, fusion and fission are parts of the same fusion-fission reactions, whereas in many approaches these three stages are studied separately. One example of such an approach is the calculation within the quantum diffusion approach (see [1] and references therein) of the capture probability, where the partial capture probability is defined by the probability of passing the potential barrier in the relative distance coordinate at fixed value of the angular momentum. Another example is the concept of a dinuclear system (DNS) [2–5]. In this model it is assumed that after the touching point both target and projectile keep their "individuality" that is, both their spherical shape and shell structure. The entrance channel in this model is taken into account through the formation probability of the DNS, which is calculated on the basis of the optical model, but this is the only memory of the entrance channel. So, the initial stage and the further evolution of the system are carried out within very different approaches.

More consistent are the approaches developed in [6–10]. The parameters of the entrance channel (the dependence of the compound-nucleus formation probability on the angular moment) [8] and the further evolution of the composite system [6] are considered within the same approach. However, whereas the DNS approach starts from the contact of the two nuclei, in [6,7] this moment is missing completely. Once the probability for the compound nucleus formation is known, the evolution of the fissioning system starts from the ground state. Thus the "prehistory" is ignored completely. In this way a considerable portion of the information about the system's evolution is lost.

In [11,12] the authors suggested considering the approach phase, fusion, and fission within the same framework.

In [11] and subsequent papers [13–16] of these authors the whole process is divided into three steps. The first two steps (approach process and fusion) are considered within a dynamical approach, namely, by solving the Langevin equations for

*vlad.lit@bk.ru
†pashkevi@theor.jinr.ru
‡kosenko@phys.omsu.omskreg.ru
§ivanyuk@kinr.kiev.ua

the variables which specify the shape of the composite system. The last step is the statistical decay of the compound nucleus. Such an approach allows for the calculation of the fission probability and saves a lot of computation time. However, details of the decay of the compound nucleus, such as the energy and mass distribution of the fission fragments, cannot be described within the statistical approach.

The two steps for the fusion process introduced in [11] are the approach of the ions up to the touching point and the overcoming of the conditional saddle or the ridge line.

The second step of the two-step model [11] for fusion could be applied to the fissionlike process (fast fission or quasifission) *without* passing through a compound nucleus, though there appears no explicit applications to those processes, probably due to the stronger interest in the synthesis of superheavy elements, i.e., in the probability for the formation of the compound nucleus.

In [12] the authors suggested combining the overcoming of the ridge line and the fission from inside the saddle into one stage for the evolution of the compact system and describing the evolution of the compact system in the same way as the approach phase using Langevin equations.

The application of Langevin equations makes possible a detailed description of reactions with heavy ions—including deep-inelastic collisions, quasifission, fission of spherical or deformed compact systems, and formation of the evaporation residue leading to the synthesis of superheavy elements—and of energy and mass distributions of the fission (or quasifission) fragments.

In the suggested model [12] the description of fusion-fission reactions is split into two stages: first, the approach of the bombarding ion (projectile) to the target nucleus up to the touching point and, second, the evolution of the monosystem formed after the touching of projectile and target nuclei. In the first stage the distance between the centers of mass of the two ions and their quadrupole deformations were taken into account. In the second stage the shape of the compact system is described in terms of distorted Cassinian ovaloids with three parameters which specify the overall elongation of the system, the mass asymmetry, and the neck radius. Both reaction stages are described within the same dynamical approach, namely, by means of Langevin equations for the parameters specifying the shape of the separated or compact system. The stochastic features of the process are taken into account by a random force term in the Langevin equations.

In the present work we continue to work within the approach of [12]. In the first formulation of the model [12] the deformation energy of the colliding nuclei was calculated within a pure liquid-drop model, so that shell and pairing effects were neglected. It is well known, however, that shell and pairing effects have a major influence on the formation of the fission fragments. It is important, therefore, to investigate the effect of the shells of the colliding ions on the evolution of the compound system.

The influence of the shell and pairing effects in the deformation energy on the properties of the system at the touching point was investigated in [17]. There, pairs of projectile and target nuclei, which are spherical (^{18}O + ^{208}Pb → ^{226}Th) or deformed (^{100}Mo+ ^{100}Mo → ^{200}Po) in their ground state, were examined. It was found that the account of pairing and shell effects modifies considerably the properties of the combined system at the touching point for both types of reactions.

The purpose of the present work is to study the consequences of the account of the shell structure of the colliding ions on the second stage of fusion-fission reactions. Here we consider target and projectile nuclei, which are spherical in their ground state. The calculated distributions for the reaction ^{18}O + ^{208}Pb → ^{226}Th are compared with those presented in [12] (i.e., liquid-drop deformation energy in the entrance channel). The calculated results for the reactions ^{16}O + ^{208}Pb → ^{224}Th and ^{48}Ca+ ^{208}Pb → ^{256}No are compared with the experimental data published in [18–23] and [24,25], respectively.

II. THE REACTION MODEL

We define the shape of the colliding ions and of the compact system by the parametrization developed in [26,27]. In this parametrization the lemniscate coordinate system $\{R, x\}$ is used. The coordinates $\{R, x\}$ are related to some cylindrical coordinates $\{\overline{\rho}, \overline{z}\}$ using the equations

$$\begin{aligned} \overline{\rho} &= \frac{1}{\sqrt{2}}\sqrt{p(x) - R^2(2x^2-1) - s}, \\ \overline{z} &= \frac{\mathrm{sign}(x)}{\sqrt{2}}\sqrt{p(x) + R^2(2x^2-1) + s}, \\ p^2(x) &\equiv [R^4 + 2sR^2(2x^2-1) + s^2], \\ 0 &\leqslant R \leqslant \infty, -1 \leqslant x \leqslant 1. \end{aligned} \tag{1}$$

The coordinate surfaces of the lemniscate system $R(x) = R_0$ are the Cassini ovaloids with $s \equiv \varepsilon R_0^2$, where s is the squared distance between the focus of Cassinian ovals and the origin of the coordinate system. The spherical shape of the nucleus corresponds to $\varepsilon = 0$. For $0 < \varepsilon < 0.4$ the Cassinian ovals are very close to ellipses with the ratio of half-axes equal to $(1 - 2\varepsilon/3)/(1 + \varepsilon/3)$. At larger ε values a neck appears and the neck radius turns to zero at $\varepsilon = 1$.

The deviation of the nuclear surface from Cassini ovaloids is defined by a series expansion of $R(x)$ in Legendre polynomials $P_n(x)$,

$$R(x) = R_0\left[1 + \sum_n \alpha_n P_n(x)\right], \tag{2}$$

where $R_0 = r_0 A^{1/3}$ is the radius of the spherical nucleus with the same volume, with $r_0 = 1.25$ fm. The volume conservation condition is fulfilled by the scaling of the cylindrical coordinates $\{\overline{\rho}, \overline{z}\}$, namely,

$$\overline{\rho} \to \rho \equiv \overline{\rho}/c, \quad \overline{z} \to z \equiv (\overline{z} - \overline{z}_{\mathrm{c.m.}})/c, \quad c = (V/V_0)^{1/3}, \tag{3}$$

where V and V_0 are the volumes of the deformed and spherical nuclei, respectively, and $\overline{z}_{\mathrm{c.m.}}$ is the z coordinate of the center of mass of the Cassini ovaloid.

The parameters ε and α_n are considered as the deformation parameters. Instead of using ε, it turns out to be convenient to introduce another parameter, α, which is defined so that at

$\alpha = 1$ the neck radius becomes zero for any choice of the other deformation parameters $\{\alpha_n\}$,

$$\varepsilon = \frac{\alpha-1}{4}\left\{(1+\sum_n \alpha_n)^2 + [1+\sum_n (-1)^n \alpha_n]^2\right\} + \frac{\alpha+1}{2}\left[1+\sum_n (-1)^n \alpha_{2n}(2n-1)!!/(2^n n!)\right]^2. \quad (4)$$

The time evolution of the collective degrees of freedom, $\mathbf{q} \equiv (\alpha, \alpha_n)$, and the corresponding momenta $\mathbf{p}/\mathbf{m} \equiv (\dot{\alpha}, \dot{\alpha}_n)$ at both stages of the reaction is described in terms of the Langevin equations [28,29], namely,

$$\dot{q}_\beta = \mu_{\beta\nu} p_\nu,$$
$$\dot{p}_\beta = -\frac{1}{2} p_\nu p_\eta \frac{\partial \mu_{\nu\eta}}{\partial q_\beta} + K_\beta - \gamma_{\beta\nu}\mu_{\nu\eta} p_\eta + \theta_{\beta\nu}\xi_\nu. \quad (5)$$

Here q_β are the deformation parameters and a convention of summation over repeated indices ν, η is used. The quantity $\gamma_{\beta\nu}$ is the tensor of friction coefficients and $\mu_{\beta\nu}$ is the tensor inverse to the mass tensor $m_{\beta\nu}$. The derivative of the potential energy of the system, $V_{\rm pot}$, with respect to the deformation parameters represents the conservative force, $K_\beta = -\partial V_{\rm pot}/\partial q_\beta$.

The random force $\theta_{\beta\nu}\xi_\nu$ takes into account the fluctuations in the system, where ξ_ν is a random number with the following properties:

$$\langle \xi_\nu \rangle = 0,$$
$$\langle \xi_\beta(t_1)\xi_\nu(t_2)\rangle = 2\delta_{\beta\nu}\delta(t_1 - t_2). \quad (6)$$

The magnitude of the random force $\theta_{\beta\nu}$ is expressed in terms of the diffusion tensor $D_{\beta\nu}$, $D_{\beta\nu} = \theta_{\beta\eta}\theta_{\eta\nu}$, which is related to the friction tensor $\gamma_{\beta\nu}$ via the Einstein relation $D_{\beta\nu} = T\gamma_{\beta\nu}$. Here T is the temperature related to the excitation (dissipated) energy by the Fermi-gas formula, $T = \sqrt{aE_{\rm dis}}$, with a being the level density parameter [30]. The dissipated energy $E_{\rm dis}$ is calculated at each time step of Eqs. (5) as

$$E_{\rm dis} = E_{\rm c.m.} - \frac{1}{2}\sum_{\beta\nu} p_\beta p_\eta \mu_{\beta\eta} - V_{\rm pot}. \quad (7)$$

For the entrance channel the potential energy (denoted by $V^{\rm fus}$) is given by (8) and by (19) (see the following for the evolution of the monosystem).

A. The approach process

Initially, the system consists of two spherical or slightly deformed ions. We assume that the ions are oriented "nose to nose"; i.e., their symmetry axes coincide. This assumption is, of course, a simplification, but it allows for the calculation of the interaction energy and of the shell contribution to the deformation energy of the colliding ions without lengthy computations. Moreover, we assume that the shape of the ions in the entrance channel is well described by Cassini ovaloids (1); i.e., the shape of each ion can be specified by one deformation parameter α.

Thus, in the entrance channel the system is characterized by three collective parameters, namely, $\alpha_{\rm t}$, $\alpha_{\rm p}$, and r, where $\alpha_{\rm t}$ and $\alpha_{\rm p}$ are the deformation parameters of target and projectile nuclei and r is the distance between their centers of mass.

The potential energy of such a system consists of the Coulomb energy $V_{\rm Coul}$, the nuclear interaction energy $V_{\rm GK}$, the rotational energy, and the deformation energy $E_{\rm def}^{\rm (t,p)}$ of target and projectile nuclei,

$$V^{\rm fus} = V_{\rm Coul} + V_{\rm GK} + \frac{\hbar^2 L^2}{2(Mr^2 + J_{\rm t} + J_{\rm p})} + \sum_{\rm t,p} E_{\rm def}^{\rm (t,p)}. \quad (8)$$

Here M is the reduced mass of the system and $J_{\rm t,p}$ are the rigid-body moments of inertia of the target and projectile nuclei [31]. The moments of inertia were calculated within the assumption of a sharp density distribution. The shell correction δJ to the rigid-body moment of inertia is very small, $\delta J/J \approx 10^{-2} \div 10^{-3}$ [32], and can be neglected.

For the nuclear interaction between target and projectile nuclei we use a modified version of the Gross-Kalinowski potential [33], which was introduced originally to specify the interaction between spherical nuclei and was modified later [34] for the case of deformed nuclei, i.e.,

$$V_{\rm GK} = \tfrac{1}{2}G(V_{12} + V_{21}), \quad (9)$$

where the value of the constant G depends on the curvatures of both nuclear surfaces and

$$V_{ij} = \int V_i(\mathbf{r} - \mathbf{r}', \alpha_i)\rho_j(\mathbf{r}', \alpha_j)\, d\mathbf{r}'. \quad (10)$$

The nucleon-nucleus potential V_i is of Woods-Saxon type, namely,

$$V_i(\mathbf{r}, \alpha_i) = V_p\left[1 + \exp\left(\frac{r - R_p(\alpha_i, z)}{a_p}\right)\right]^{-1}, \quad (11)$$

with parameters V_p and a_p taken from [34] and with the radius parameter $R_p(\alpha, z) = R_0\sqrt{\rho^2(\alpha, z) + z^2}$, where the profile function $\rho(\alpha, z)$ is defined by (1)–(4). The nuclear density is chosen in the following form:

$$\rho_i(\mathbf{r}, \alpha_i) = \rho_0\left[1 + \exp\left(\frac{r - R_d(\alpha_i, z)}{a_d}\right)\right]^{-1}, \quad (12)$$

where $\rho_0 = 0.17$ fm^{-3}, the density diffuseness parameter $a_d = 0.54$ fm, and $R_d(\alpha, z) = (1.25A^{1/3} - 0.86A^{-1/3})\sqrt{\rho^2(\alpha, z) + z^2}$ fm.

The deformation energy of the colliding nuclei is calculated within the macroscopic-microscopic method [35,36]. In this method the deformation energy is expressed as the sum of the macroscopic part (liquid-drop energy) and the shell correction $E_{\rm shell}$ (including the shell correction to the pairing correlation energy), i.e.,

$$E_{\rm def} = E_{\rm def}^{\rm LDM} + E_{\rm shell}. \quad (13)$$

For the macroscopic part we used the liquid-drop model with the parameters given in [37]. The shell correction for protons (p) and neutrons (n) is calculated using the Strutinsky method [35,36]:

$$E_{\rm shell}(T = 0) = \sum_{\rm p,n}(\delta E^{\rm p,n} + \delta P^{\rm p,n}). \quad (14)$$

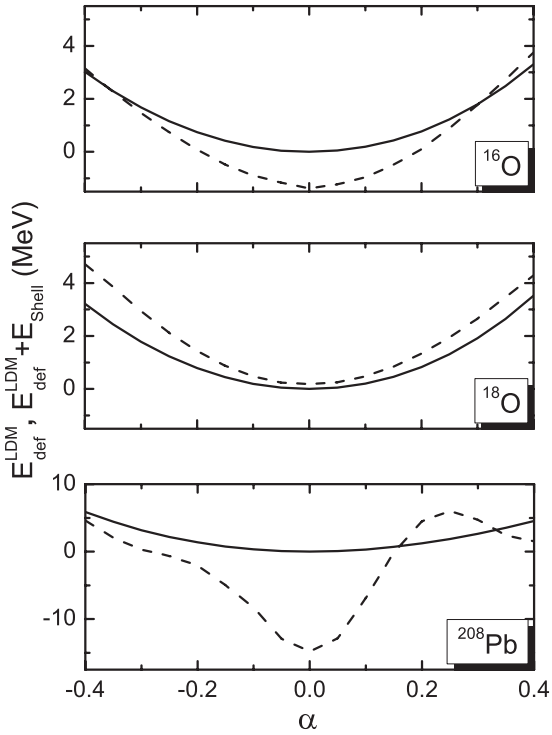

FIG. 1. The liquid-drop (solid) and the total (dashed) deformation energy of ^{16}O, ^{18}O, and ^{208}Pb nuclei as a function of the deformation parameter α.

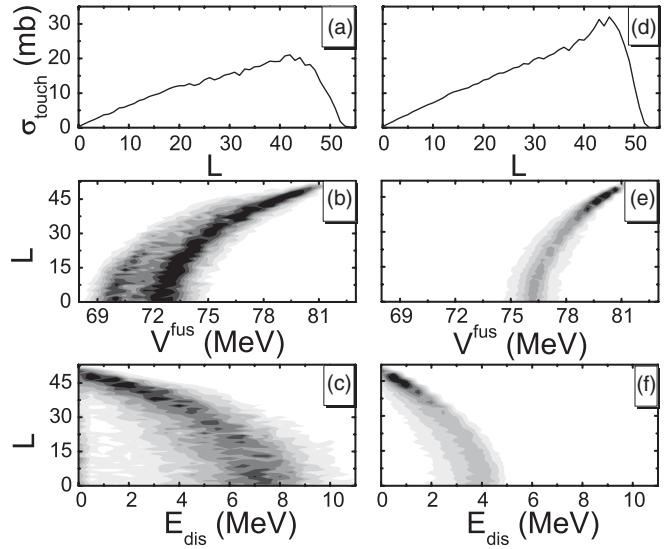

FIG. 2. Characteristics of the system at the touching point for the reaction $^{18}\mathrm{O} + ^{208}\mathrm{Pb} \rightarrow ^{226}\mathrm{Th}$, at the center-of-mass energy $E_{\mathrm{c.m.}} = 82$ MeV. Panels (a), (b), and (c) show the quantities calculated with the liquid-drop deformation energy, and (d), (e), and (f) show those with the shell correction taken into account. Panels (a) and (d) show the dependence of the touching cross section on the angular momentum L, panels (b) and (e) display the distribution of the touching events in the potential energy and the angular momentum, and panels (c) and (f) show the distribution of the touching events in the dissipated energy and the angular momentum.

The dependence of the shell correction on the temperature is given by the expression $E_{\mathrm{shell}}(T) = E_{\mathrm{shell}}(T=0)e^{-a\gamma T^2}$ [38]. The level density parameter a and the shell correction damping parameter γ are taken from [30]. The comparison of the liquid drop and the total deformation energy (13) for a few nuclei is shown in Fig. 1. One can see that the shell correction modifies substantially the stiffness of the potential energy and, as a result, the ability of the ions to get deformed during the approach phase.

In order to specify the coefficients of the Langevin equation completely one would need also the friction and inertia tensors. The friction tensor in the entrance channel is chosen in the same form as in [34], namely,

$$\gamma_{rr}^{\mathrm{fus}} = \gamma_0 \, (dV_{\mathrm{GK}}/dr)^2 \, ,$$
$$\gamma_{ri}^{\mathrm{fus}} = -\frac{1}{2}\gamma_{rr}^{\mathrm{fus}} \frac{R_{i0}}{\sqrt{\alpha_i + 1}} \left(\frac{c_i - 2(\alpha_i + 1) dc_i/d\alpha_i}{c_i^2} \right) , \qquad (15)$$
$$\gamma_{ij}^{\mathrm{fus}} = \gamma_{ri}^{\mathrm{fus}} \gamma_{rj}^{\mathrm{fus}} \big/ \gamma_{rr}^{\mathrm{fus}} + \delta_{ij}\gamma_{ij},$$

where indices i and j refer to α_{t} and α_{p}, whereas the index r corresponds to the distance between the centers of mass of target and projectile nuclei. Here we use the coefficient $\gamma_0 = 4 \times 10^{-23}$ s MeV^{-1}, with the radii R_{i0} of the corresponding spherical nuclei, and the scaling factors c_i is introduced to ensure volume conservation during deformation.

The inertia tensor in the entrance channel is diagonal. Its rr component is simply the reduced mass $m_{rr}^{\mathrm{fus}} = M$ and its $\alpha_{\mathrm{t}}\alpha_{\mathrm{t}}$ and $\alpha_{\mathrm{p}}\alpha_{\mathrm{p}}$ components are calculated in the same way as for the compact system, $m_{\alpha_{\mathrm{t}}\alpha_{\mathrm{t}}}^{\mathrm{fus}} = m_{\alpha_{\mathrm{t}}\alpha_{\mathrm{t}}}$ and $m_{\alpha_{\mathrm{p}}\alpha_{\mathrm{p}}}^{\mathrm{fus}} = m_{\alpha_{\mathrm{p}}\alpha_{\mathrm{p}}}$, as given in Eq. (17) below.

The friction γ_{ij} and inertia m_{ij} tensors for the deformation degrees of freedom are defined within the linear response approach and the locally harmonic approximation [39,40]. The widely used wall-and-window formula for the friction tensor [41] and the Werner-Wheeler approximation [42] for the mass tensor are *macroscopic* approximations. They are justified either for large systems or at high enough excitation energy (temperature). The use of these approximations for the fusion-fission reactions when the energies of the incoming ions are comparable with the height of the Coulomb barrier is very questionably. At such energies microscopic effects come into play.

For comparison [see Fig. 2(a)–2(c)], we have carried out also some calculations with macroscopic friction and mass tensors, as was done in the first formulation of the model [12].

The linear response approach using the locally harmonic approximation [39,40] for the transport coefficients is based on a microscopic Hamiltonian. In this approach, many quantum effects, such as shell and pairing effects and the dependence of the collisional width of single-particle states on the excitation energy, are taken into account. The two main ingredients of this approach are the mean-field Hamiltonian and the collisional width of single-particle states. For the mean-field Hamiltonian we use here the shell-model Hamiltonian with a deformed Woods-Saxon potential [26,27]. The parameters of this potential were fitted to reproduce the fission barriers of heavy nuclei. For the collisional width a well-known expression from Fermi-liquid theory is used.

The parameters which appear in this expression were fitted long ago to the data on the nucleon effective mass and the width of giant resonances [39]. It was demonstrated in Ref. [43] that the reduced friction coefficient γ/M calculated within the linear response approach is in quite good agreement with the experimental data extracted from the fission experiments [44].

The precise expressions for the friction γ_{ij} and inertia m_{ij} tensors can be found in [45]. They are

$$\gamma_{ij}/\hbar = 2\sum_{kl}\left(n_k^T - n_l^T\right)\xi_{kl}^2 \frac{E_{kl}^- \Gamma_{kl}}{\left[(E_{kl}^-)^2 + \Gamma_{kl}^2\right]^2} F_i^{kl} F_j^{lk} + 2\sum_{kl}\left(n_k^T + n_l^T - 1\right)\eta_{kl}^2 \frac{E_{kl}^+ \Gamma_{kl}}{\left[(E_{kl}^+)^2 + \Gamma_{kl}^2\right]^2} F_i^{kl} F_j^{lk} \tag{16}$$

and

$$m_{ij}/\hbar^2 = \sum_{kl}\left(n_k^T - n_l^T\right)\xi_{kl}^2 \frac{(E_{kl}^-)^2(E_{kl}^- - 3\Gamma_{kl})}{\left[(E_{kl}^-)^2 + \Gamma_{kl}^2\right]^3} F_i^{kl} F_j^{lk} + \sum_{kl}\left(n_k^T + n_l^T - 1\right)\eta_{kl}^2 \frac{(E_{kl}^+)^2(E_{kl}^+ - 3\Gamma_{kl})}{\left[(E_{kl}^+)^2 + \Gamma_{kl}^2\right]^3} F_i^{kl} F_j^{lk}. \tag{17}$$

Here E_k and E_l are the quasiparticle energies in the BCS approximation, $E_{kl}^- \equiv E_k - E_l$, $E_{kl}^+ \equiv E_k + E_l$, $n_k^T \equiv 1/[1 + \exp(E_k/T)]$, $\eta_{kl} = u_k v_l + u_l v_k$, and $\xi_{kl} = u_k u_l - v_k v_l$, where u_k and v_k are the coefficients of the Bogolyubov-Valatin transformation. In (16) and (17) the summation is carried out over single-particle states $|k\rangle$ and $|l\rangle$. The operator $\hat{F}_j$, which appears in (16) and (17), is the derivative of the nuclear Hamiltonian in the BCS approximation with respect to the deformation parameter α_j. The quantity Γ_{kl} is the average width of the two-quasiparticle states, $\Gamma_{kl} = [\Gamma(E_k, \Delta, T) + \Gamma(E_l, \Delta, T)]/2$. The calculation of Γ_{kl} for a system with pairing correlations is explained in detail in [46].

The Langevin equations (5) are integrated starting from the initial distance $r_{\text{in}} = 4R_{\text{touch}}$. The touching point R_{touch} was defined in [12] as $R_{\text{touch}} = R_1 + R_2 + (a_{d,\text{t}} + a_{d,\text{p}})/2$, where R_1 and R_2 are the nuclear radii along their common symmetry axes, and the third term accounts for the diffuseness of the density distributions [33]. We have checked that the increase of r_{in} does not significantly change the results of calculations but does increase the computation time substantially.

Besides r_{in}, at the initial moment we fix the value of the angular momentum L and choose the random number ξ_ν which appears in the random force $\theta_{\beta\nu}\xi_\nu$ (5). The random force means that, at the touching point, rather than fixed quantities we get distributions. Changing the initial value of ξ_ν, we repeated the calculations many times, up to 10^5, until the results were stable with respect to the number of trajectories. By trajectory, we mean here the dependence of r on time for a given calculation.

Equations (5) are integrated until the trajectory $r(t)$ reaches the touching point R_{touch} or returns to the starting point r_{in}. As was illustrated in [47], due to the random force a certain number of trajectories cannot reach the touching point even if they overcome the fusion barrier.

From the calculations of the first stage we get the touching probability and its dependence on the angular momentum L and the distributions of the potential and the dissipated energy, as illustrated in Fig. 2. We define the touching probability $T(L)$ as the ratio of the number of trajectories, $N_{L,\text{touch}}$, which have reached the touching point, relative to the total number of trajectories, N_L, under consideration, $T(L) = N_{L,\text{touch}}/N_L$. Knowing this probability one can readily find the partial and the total touching cross sections $\sigma_{\text{touch}}(L) = \pi\lambda^2(2L + 1)T(L)$ and $\sigma_{\text{touch}} = \sum_L \sigma_{\text{touch}}(L)$.

Here, a few words are in order on the use of the terms *touching cross section* and the often used *capture cross section*. By the capture process one usually means the trapping of the colliding nuclei into the well of the nucleus-nucleus potential after dissipation of part of the initial relative kinetic energy and orbital angular momentum.

By the very construction of our model, at the touching point (which is inside of the barrier of the nucleus-nucleus interaction), the incoming ion and the target nucleus form a compact system which can undergo quasifission or form a quasistationary state inside the saddle configuration and then fission from inside the saddle can occur, as seen on Fig. 5. The touching process is just the beginning of the capture process. Thus, the touching and capture cross sections should be the same or very close to each other.

Results of calculations for the first stage with and without taking into account shell effects in the deformation energy differ from each other. In the case of nuclei that are spherical in the ground state, the main reason for this difference is the increasing stiffness of the potential energy due to the shell effects (see Fig. 1). The larger is the stiffness, the less deformed are the ions at the touching point. On the other hand, the deformation of the ions in the approach phase reduces the potential energy; i.e., the smaller is the stiffness, the more favorable is the shape of colliding ions at the touching point. These speculations are confirmed by the numerical results shown in Fig. 2. The distribution calculated with shell effects taken into account is narrower and the average value of the potential energy at the touching point is approximately 4 MeV larger than that in the pure *liquid-drop* case.

In Fig. 3 we compare the experimental values of fusion cross sections σ_{fus} and the calculated touching cross sections σ_{touch} for the reactions $^{16,18}\text{O} + ^{208}\text{Pb} \rightarrow ^{224,226}\text{Th}$. Since not all touching events lead to fusion, the touching cross sections should be larger than the fusion cross section. Indeed, at high energies, the σ_{touch} value is larger than that of σ_{fus}. However, this is not the case for lower energies (at the fusion barrier and below).

To solve this problem the authors of Ref. [47] suggested taking into account quantum tunneling through the fusion barrier. The penetrability of the barrier was defined in the WKB approximation as

$$T_L(E) = \left[1 + \exp\left(\frac{2}{\hbar}\int_{r_2}^{r_1}\sqrt{2m(V^{\text{fus}} - E)}\,dr\right)\right]^{-1}, \tag{18}$$

where the integration is carried out between the turning points r_1 and r_2 in the subbarrier region and E is the potential energy of the system at the turning points. As one can see

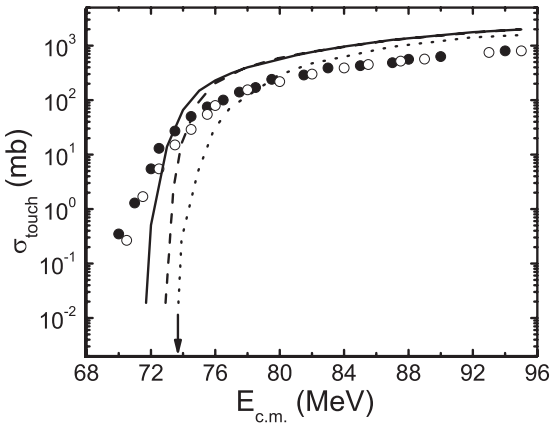

FIG. 3. The dependence of the touching cross section σ_{touch} on the center-of-mass energy $E_{c.m.}$ of the incoming ions. The calculations are done by taking into account tunneling for the reactions $^{18}O + ^{208}Pb \rightarrow ^{226}Th$ (solid) and $^{16}O + ^{208}Pb \rightarrow ^{224}Th$ (dashed). The dotted line is the calculation for the reaction $^{18}O + ^{208}Pb \rightarrow ^{226}Th$ without tunneling. The experimental values [18] for the fusion cross section for the reactions $^{18}O + ^{208}Pb \rightarrow ^{226}Th$ and $^{16}O + ^{208}Pb \rightarrow ^{224}Th$ are marked by • and ○, respectively. . The arrow shows the height of the fusion barrier (for $L = 0$) for the $^{18}O + ^{208}Pb \rightarrow ^{226}Th$ reaction.

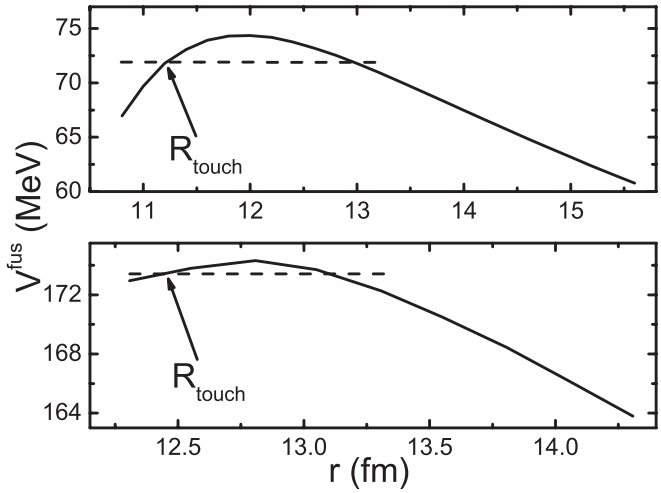

FIG. 4. The dependence of the potential energy of two separated ions on the distance r between their centers of mass for the reactions $^{18}O + ^{208}Pb \rightarrow ^{226}Th$ (top) and $^{48}Ca + ^{208}Pb \rightarrow ^{256}No$ (bottom). The dashed line shows the end of the region accessible for tunneling. The arrow shows the position of the touching point.

from Fig. 3, accounting for quantum tunneling increases the touching probability in the subbarrier region.

The comparison of the measured fusion cross sections for both reactions (see Fig. 3) shows that in the low-energy region the fusion cross section is somewhat larger for the heavier projectile, while at high energies both cross sections are practically the same.

The calculated touching cross section is also larger for heavier projectiles (and in this sense the dependence of σ_{touch} on the mass of the projectile is the same for calculated and measured cross sections), but the calculated touching cross section for ^{18}O projectiles is larger up to two orders of magnitude as compared with that for ^{16}O projectiles in the subbarrier region. The reason for this is that the calculated barrier height for the $^{18}O + ^{208}Pb \rightarrow ^{226}Th$ reaction is approximately 1 MeV lower than for the $^{16}O + ^{208}Pb \rightarrow ^{224}Th$ reaction. If one would shift the (dashed) curve of the touching cross section for heavier projectile to the left along the $E_{c.m.}$ axes in Fig. 3 then it would almost coincide with the touching cross section for the lighter projectile (solid line).

The calculated touching cross section in the low-energy region is still substantially smaller than the experimental fusion cross section (see also Fig. 7). One way to possibly overcome this difficulty could be to use a more flexible parametrization of the shape of the system (for example, by taking into account the octupole deformation of ions).

Unfortunately, accounting for the possibility of tunneling [47] is effective only for reactions with a large target and projectile mass asymmetry such as in $^{18}O + ^{208}Pb \rightarrow ^{226}Th$.

For different combinations of projectile and target nuclei the projectile energies at the touching point and at the fusion barrier are different [see Figs. 4(a) and 4(b)]. The lower is the energy of the ions at the touching point, the larger is the contribution from the tunneling effect to the fusion probability. In the case of the $^{48}Ca + ^{208}Pb \rightarrow ^{256}No$ reaction the energy of the bombarding ions at the touching point is smaller than the fusion barrier by less than 1 MeV, and the enhancement of the fusion probability by the tunneling effect is thus very small.

B. The evolution of the compact system

In the case of the reactions considered in the present paper the shape of the system just after the touching point is characterized by an increasing elongation and mass asymmetry. Such shapes can be described in terms of distorted Cassinian ovaloids (2). Thus, besides the elongation parameter α we take into account the parameters α_1 and α_4 which characterize the mass asymmetry and the neck radius.

The potential energy V_{pot} of the compact system consists of rotational and deformation energies, i.e.,

$$V_{pot} = \frac{\hbar^2 L^2}{2J} + E_{def}, \tag{19}$$

where J is the rigid-body moment of inertia [31]. The deformation energy and the friction and inertia tensors for the α, α_1, and α_4 degrees of freedom are calculated in the same way as in the entrance channel, by using the Strutinsky method and Eqs. (16) and (17), respectively.

The deformation dependence of the potential energy of the system is shown in Fig. 5. In this plot we also illustrate several different possibilities for the evolution of the shape of the compact system.

To solve the Langevin equations for the evolution of the compact system one needs initial conditions. First of all, one should define the shape of the compact system at the touching point. The parameter α is defined by keeping in mind that at the touching point both the divided and the compact system should have a small neck radius. The parameters α_1 and α_4 are

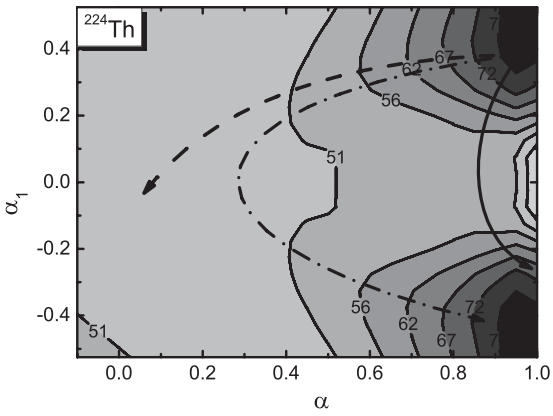

FIG. 5. The dependence of the deformation energy of the compound nucleus ^{224}Th on the deformation parameters α and α_1 for $\alpha_4 = 0$. The possible evolution of the shape of the system is shown by dashed (the formation of the evaporation residue), dash-doted (fission events), and solid (quasifission events) lines. The initial point of the calculations of the evolution of the compact system is indicated by the • symbol.

fixed by the initial mass asymmetry and by the requirement that the potential energy of the divided and compact system at the touching point be the same.

The angular momentum of the system, its potential $V_{\rm pot}$, and dissipated energy $E_{\rm dis}$ are chosen randomly by the "hit and miss" method from the distributions at the touching point, calculated in the entrance channel (see Fig. 2).

By solving the Langevin equations in the first stage we get, at the touching point, the distributions of the collective momenta p_r, p_{α_t}, and p_{α_p}. Unfortunately, it is not easy to relate these final values of p_r, p_{α_t}, and p_{α_p} to the initial values of momenta p_α, p_{α_1}, and p_{α_4} of the monosystem. So, to fix the initial momenta of the monosystem we define the kinetic energy as $E_{\rm kin} = E_{\rm c.m.} - V_{\rm pot} - E_{\rm dis}$ (which is small in the most interesting case when the kinetic energy of the incoming ions is comparable with the Coulomb barrier height) and distribute it randomly among the α, α_1, and α_4 degrees of freedom with the restriction that p_α should lead to smaller elongations, i.e., decreasing α values.

The Langevin equations (5) are integrated until the system fissions or cools down by light-particle or γ-quanta evaporation [30] and thus forms the evaporation residue. The trajectories $r(t)$ were sorted according to their minimal value $r_{\rm min}$ reached during the evolution of the compact system. A certain number of trajectories do not reach the so-called scission point $r_{\rm scission}$, which is the critical distance above which the monosystem breaks apart. It was found in [48] that $r_{\rm scission} \approx 2.35 R_0$. The trajectories which did not reach the scission point were considered as deep-inelastic collisions. The trajectories with $r_{\rm saddle} \leqslant r_{\rm min} \leqslant r_{\rm scission}$ were considered as quasifission events. Finally, the trajectories which cross the saddle point $r_{\rm min} < r_{\rm saddle}$ contribute to true fission or evaporation-residue formation. All these possibilities are shown schematically in Fig. 5. When we discuss the fission fragments distributions below we mean the true fission events, i.e., the events when the system fissions from inside the saddle.

The evaporation of particles and γ quanta by the excited compact system was described within the statistical model [30]. At each integration step, by the "hit and miss" method, we decide whether a particle was emitted and which kind of particle was emitted. If some particle was emitted, the binding energy of this particle was subtracted from the excitation energy of the system. The expressions for the partial width of the corresponding decay channel were taken from [30].

III. NUMERICAL RESULTS AND DISCUSSION

As a result of calculating the compact system evolution we obtain the distributions of the fission fragments in mass and kinetic energy, the partial (total) cross sections of the compound nucleus, $\sigma_{\rm comp}(L)$ [$\sigma_{\rm comp} = \sum_L \sigma_{\rm comp}(L)$], and of the evaporation-residue formation, $\sigma_{\rm er}(L)$ [$\sigma_{\rm er} = \sum_L \sigma_{\rm er}(L)$], and the multiplicities of evaporated particles and γ rays.

The quantities $\sigma_{\rm comp}(L)$ and $\sigma_{\rm er}(L)$ are the products of the touching cross section and the corresponding probability, $\sigma_{\rm comp}(L) = P_{\rm comp}(L)\sigma_{\rm touch}(L)$ and $\sigma_{\rm er}(L) = P_{\rm er}(L)\sigma_{\rm touch}(L)$. The probabilities $P_{\rm comp}(L)$ and $P_{\rm er}(L)$ are calculated as the ratio of the number of trajectories leading to the formation of the compound nucleus or the evaporation residue to the total number of trajectories considered at the second stage of the calculation. The total probability of evaporation-residue formation is then given by the product $P_{\rm touch} P_{\rm er}$.

In Fig. 6 we compare the experimental and calculated evaporation-residue cross section $\sigma_{\rm er}$ for the reaction $^{16}{\rm O} + {}^{208}{\rm Pb} \rightarrow {}^{224}{\rm Th}$. As one can see, the experimental data [18–21] differ from each other by up to one order of magnitude. The data presented in [20] and [21] are the most recent and seem to be the most reliable. Like in the case of the touching cross section, the calculated evaporation-residue cross section $\sigma_{\rm er}$ is close to the experimental values in the high-energy region and smaller by up to two orders of magnitude for near-barrier

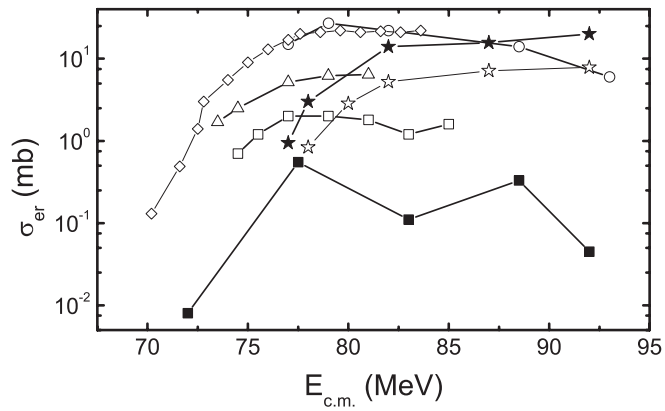

FIG. 6. The dependence of the evaporation residue cross section $\sigma_{\rm er}$ on the center-of-mass energy $E_{\rm c.m.}$ of bombarding ions. The experimental data for the reaction $^{16}{\rm O} + {}^{208}{\rm Pb}$ are taken from [18] (□), [19] (◯), [20] (▽), and [21] (◇). The black squares (■) show the cross section calculated in [12] for the reaction $^{18}{\rm O} + {}^{208}{\rm Pb}$ with shell effects in the deformation energy neglected. The presently calculated cross sections $\sigma_{\rm er}$ for the reactions $^{16}{\rm O} + {}^{208}{\rm Pb}$ and $^{18}{\rm O} + {}^{208}{\rm Pb}$ are shown by open stars and solid stars (★), respectively.

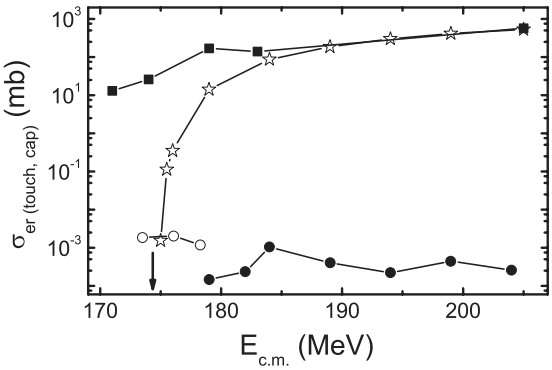

FIG. 7. The dependence of the calculated touching cross section σ_{touch} (open stars) and the evaporation residue cross section (•) on the center-of-mass energy $E_{c.m.}$ of the bombarding ions for the reaction $^{48}Ca + ^{208}Pb \rightarrow ^{256}No$. The experimental data for the capture cross section σ_{cap} are marked as ■ [25], the experimental data for σ_{er} (○) are taken from [24]. The arrow indicates the height of the fusion barrier.

energies. In Fig. 6 we compare also the calculated values of σ_{er} for the reaction $^{18}O+^{208}Pb \rightarrow ^{226}Th$ with the one calculated in [12] without shell corrections to the deformation energy taken into account. One can see that shell effects lead to an increase of σ_{er} by one or two orders of magnitude.

The calculated values of the touching σ_{touch} and evaporation-residue σ_{er} cross sections for the reaction $^{48}Ca + ^{208}Pb \rightarrow ^{256}No$ are shown in Fig. 7 . The comparison of calculated σ_{touch} and experimental cross sections in the low-energy region shows the same problem as in the case of the $^{16,18}O + ^{208}Pb \rightarrow ^{224,226}Th$ reactions. The calculated touching cross section for the near-barrier energies is too small. The experimental data for σ_{er} (open circles) are available only for energies near the fusion barrier, a region we cannot describe within the present model. We can only mention that the extrapolation of the calculated results for σ_{er} down to the subbarrier region is very close to the experimental data.

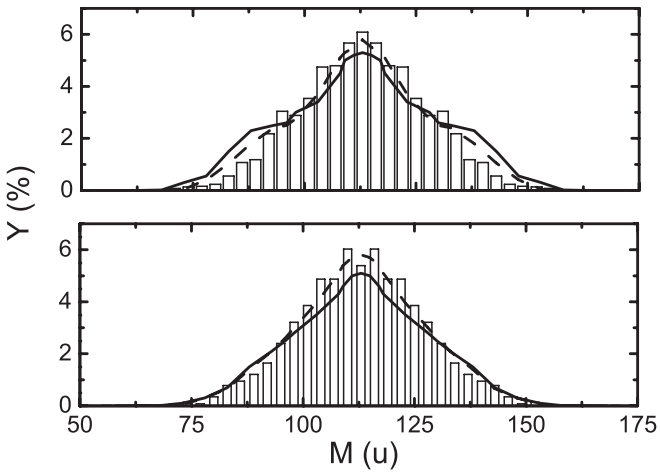

FIG. 8. The yield of the fission fragments Y (normalized to 200%) in the reaction $^{18}O + ^{208}Pb \rightarrow ^{226}Th$ for $E_{c.m.} = 72$ MeV (top) and $E_{c.m.} = 83$ MeV (bottom). The experimental data are taken from [23] (solid) and [22] (dashed). The calculated values are shown by the histogram.

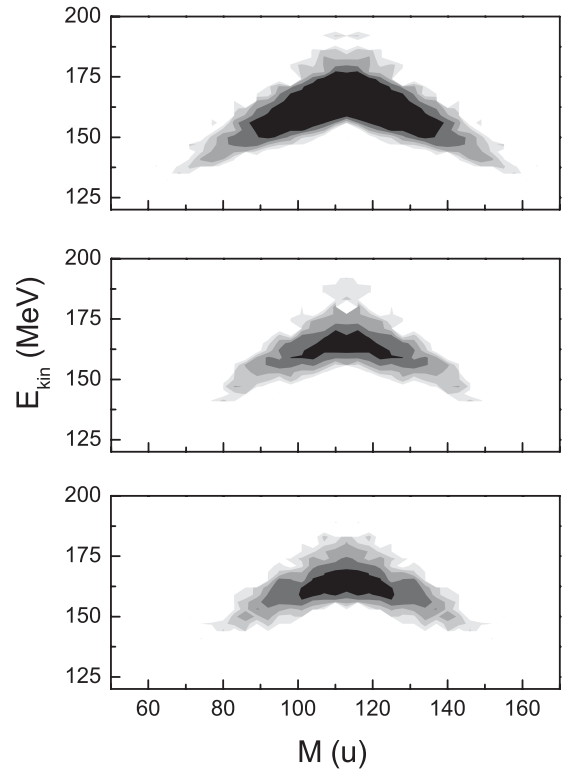

FIG. 9. Mass-energy distribution of fission fragments in the reaction $^{18}O + ^{208}Pb \rightarrow ^{226}Th$ at energy $E_{c.m.} = 72$ MeV (bottom), $E_{c.m.} = 83$ MeV (middle), and $E_{c.m.} = 107.7$ MeV (top).

We have also calculated the mass yield (see Fig. 8) and mass–kinetic energy fission-fragments distribution (see Fig. 9) for the reaction $^{18}O + ^{208}Pb \rightarrow ^{226}Th$. The calculated mass yields for the energies $E_{c.m.} = 72$ MeV and $E_{c.m.} = 83$ MeV are in good agreement with the available experimental data.

The distribution of fission fragments in mass and kinetic energy (see Fig. 9) is in agreement with the experimental data (see Fig. 1 of [23]) and is very close to that obtained in [12] (the liquid-drop deformation energy in the entrance channel). This result is consistent with the idea that the compound nucleus "does not remember" its history.

IV. CONCLUSIONS

The performed theoretical investigation of the fusion-fission reactions between nuclei which are spherical in their ground state has shown that the account of shell effects in the deformation energy of the colliding nuclei has a substantial influence on the characteristics of the combined system at the touching point as well as on the probability of evaporation-residue formation.

For the examples of $^{16,18}O + ^{208}Pb \rightarrow ^{224,226}Th$ and $^{48}Ca + ^{208}Pb \rightarrow ^{256}No$ reactions it is shown that the earlier suggested two-stage model of the fusion-fission reactions reproduces reasonably well the experimental data on the evaporation-residue cross sections for energies of the incoming ions larger than the fusion barrier. For near-barrier energies the

calculated touching or evaporation-residue cross sections are smaller than the experimental values by one or two orders of magnitude. One possible way to overcome this difficulty of the present model could be to use a more flexible parametrization of the shape of the system in the approach stage.

We have also found out that taking into account quantum tunneling through the barrier improves the agreement with experimental results only for reactions with large initial mass asymmetry.

ACKNOWLEDGMENTS

The authors are grateful to Prof. J. Bartel for helpful discussions.

[1] V. V. Sargsyan, G. G. Adamian, N. V. Antonenko, W. Scheid, and H. Q. Zhang, Phys. Rev. C **84**, 064614 (2011).
[2] N. V. Antonenko, E. A. Cherepanov, A. K. Nasirov, V. P. Permjakov, and V. V. Volkov, Phys. Lett. B **319**, 425 (1993).
[3] G. G. Adamian, A. K. Nasirov, N. V. Antonenko, and R. V. Jolos, Phys. Part. Nucl. **25**, 583 (1994).
[4] G. G. Adamian, N. V. Antonenko, and R. V. Jolos, Nucl. Phys. A **584**, 205 (1995).
[5] A. Diaz-Torres, G. G. Adamian, N. V. Antonenko, and W. Scheid, Phys. Rev. C **64**, 024604 (2001).
[6] I. I. Gontchar, Phys. Part. Nucl. **26**, 394 (1995).
[7] K. Pomorski, B. Nerlo-Pomorska, A. Surowiec, M. Kowal, J. Bartel, K. Dietrich, J. Richert, C. Schmitt, B. Benoit, E. de Goes Brennand, L. Donadille, and C. Badimon, Nucl. Phys. A **679**, 25 (2000).
[8] P. Fröbrich, J. Marten, Nucl. Phys. A **545**, 854 (1992).
[9] P. Fröbrich and S. Y. Xu., Nucl. Phys. A **477**, 143 (1988).
[10] P. Fröbrich and G. Grawert, Nucl. Phys. A **451**, 338 (1986).
[11] G. I. Kosenko, C. Shen, and Y. Abe, J. Nucl. Radiochem. Sci. **3**, 19 (2002); C. Shen, G. Kosenko, and Y. Abe, Phys. Rev. C **66**, 061602(R) (2002).
[12] G. I. Kosenko, F. A. Ivanyuk, and V. V. Pashkevich, J. Nucl. Radiochem. Sci. **3**, 71 (2002).
[13] Y. Abe *et al*., Prog. Theor. Phys. Suppl. **146**, 104 (2002).
[14] Y. Abe, D. Boilley, G. Kosenko, and C. Shen, Acta Phys. Pol. B **34**, 2091 (2003).
[15] Y. Abe, C. Shen, G. Kosenko, and D. Boilley, Phys. At. Nucl. **66**, 1057 (2003).
[16] Y. Abe, A. Marchix, C. Shen, B. Yilmaz, G. Kosenko, D. Boilley, and B. G. Giraud, Int. J. Mod. Phys. E **16**, 491 (2007).
[17] V. L. Litnevsky, G. I. Kosenko, F. A. Ivanyuk, and V. V. Pashkevich, Phys. At. Nucl. **74**, 659 (2011).
[18] E. Vulgaris, L. Grodzins, S. G. Steadman, and R. Ledoux, Phys. Rev. C **33**, 2017 (1986).
[19] K. Hartel, Ph.D. thesis, Technical University, Munich, 1985.
[20] K.-T. Brinkmann, A. L. Caraley, B. J. Fineman, N. Gan, J. Velkovska, and R. L. McGrath, Phys. Rev. C **50**, 309 (1994).
[21] C. R. Morton *et al*., Phys. Rev. C **52**, 243 (1995).
[22] I. V. Pokrovski *et al*., in *Proceedings of the International Conference on Nuclear Physics "Nuclear Shells–50," Dubna, Russia, 21–24 April* 1999, edited by Yu. Ts. Oganessian and R. Kolpakchieva (World Scientific, Singapore, 2000), p. 105.
[23] A. Ya. Rusanov, M. G. Itkis, N. A. Kondratiev, V. V. Pashkevich, I. V. Pokrovsky, S. V. Salamatin, and G. G. Chubarian, Phys. At. Nucl. **71**, 956 (2008).
[24] Yu. Ts. Oganessian *et al*., Phys. Rev. C **64**, 054606 (2001).
[25] A. J. Pacheco *et al*., Phys. Rev. C **45**, 2861 (1992).
[26] V. V. Pashkevich, Nucl. Phys. A **169**, 275 (1971).
[27] V. V. Pashkevich, Nucl. Phys. A **477**, 1 (1988).
[28] Y. Abe, S. Ayik, P.-G. Reinhard, and E. Suraud, Phys. Rep. **275**, 49 (1996).
[29] J. Marten and P. Fröbrich, Nucl. Phys. A **545**, 854 (1992).
[30] A. S. Iljinov, M. V. Mebel, N. Bianchi, E. De Sanctis, C. Guaraldo, V. Lucherini, V. Muccifora, E. Polli, A. R. Reolon and, P. Rossi, Nucl. Phys. A **543**, 517 (1992).
[31] R. W. Hasse and W. D. Myers, *Geometrical Relationships of Macroscopic Nuclear Physics* (Springer-Verlag, Heidelberg, 1988).
[32] A. G. Magner, A. M. Gzhebinsky, A. S. Sidtikov, A. A. Khamzin, and J. Bartel, Int. J. Mod. Phys. E **19**, 735 (2010).
[33] D. H. E. Gross and H. Kalinowski, Phys. Rep. **45**, 175 (1978).
[34] P. Fröbrich, Phys. Rep. **116**, 337 (1984).
[35] V. M. Strutinsky, Nucl. Phys. A **95**, 420 (1967); **122**, 1 (1968).
[36] M. Brack, J. Damgaard, A. S. Jensen, H. C. Pauli, V. M. Strutinsky, and C. Y. Wong, Rev. Mod. Phys. **44**, 320 (1972).
[37] W. D. Myers and W. J. Swiatecki, Ark. Fys. **36**, 343 (1967).
[38] A. V. Ignatyuk, G. N. Smirenkin, and A. S. Tishin, Sov. J. Nucl. Phys. **21**, 255 (1975).
[39] H. Hofmann, Phys. Rep. **284**, 137 (1997).
[40] H. Hofmann, *The Physics of Warm Nuclei with Analogies to Mesoscopic Systems* (Oxford University Press, New York, 2008).
[41] J. Blocki, Y. Boneh, J. R. Nix, J. Randrup, M. Robel, A. J. Sierk, and W. J. Swiatecki, Ann. Phys. (NY) **113**, 330 (1978).
[42] K. T. R. Davis, A. J. Sierk, and J. R. Nix, Phys. Rev. C **13**, 2385 (1976).
[43] F. A. Ivanyuk, H. Hofmann, V. V. Pashkevich, and S. Yamaji, Phys. Rev. C **55**, 1730 (1997).
[44] D. Hilscher, I. I. Gontchar, and H. Rossner, Phys. At. Nucl. **57**, 1187 (1994).
[45] F. A. Ivanyuk, in *Proceedings of International Conference on Nuclear Physics* "*Nuclear Shells–50,*" *Dubna, Russia, 21–24 April,* 1999, edited by Yu. Ts. Oganessian and R. Kolpakchieva (World Scientific, Singapore, 2000), p. 456.
[46] F. A. Ivanyuk and H. Hofmann, Nucl. Phys. A **657**, 19 (1999).
[47] T. I. Nevzorova and G. I. Kosenko, Phys. At. Nucl. **71**, 1373 (2008).
[48] F. A. Ivanyuk, Int. J. Mod. Phys. E **18**, 879 (2009).